RESEARCH ARTICLE

Excitation-Wavelength-dependent Functionalities of Temporally-controlled Sensing and Generation of Singlet Oxygen by a Photoexcited State Engineered Rhodamine 6G-anthracene Conjugate

Hanjun Zhao[a], Yuta Takano [a,b]*, Devika Sasikumar[a,b], Yukiko Miyatake[c], and Vasudevanpillai Biju [a,b]*

[a] Mr. H. Zhao, Dr. D. Sasikumar, Prof. Dr. Y. Takano, Prof. Dr. V. Biju
Graduate School of Environmental Science
Hokkaido University
N10, W5, Sapporo, 060-0810 (Japan)
E-mail: tak@es.hokudai.ac.jp, biju@es.hokudai.ac.jp
[b] Prof. Dr. Y. Takano, Prof. Dr. V. Biju
Research Institute for Electronic Science
Hokkaido University
N20, W10, Sapporo, 001-0020 (Japan)
[c] Dr. Y. Miyatake
Department of Pathology, Faculty of Medicine and Graduate School of Medicine
Hokkaido University
N15, W7, Sapporo, 060-8638 (Japan)

Supporting information for this article is given via a link at the end of the document.

Abstract: The present study provides design guidance for unique multipotent molecules that sense and generate singlet oxygen ($^1O_2$). A rhodamine 6G-aminomethylanthracene-linked donor-acceptor molecule (**RA**) is designed and synthesized for demonstrating wavelength-dependent functionalities as follows; (i) **RA** acts as a conventional fluorogenic $^1O_2$ sensor molecule like the commercially available reagent, singlet oxygen sensor green (SOSG), when it absorbs ultraviolet (UV)-visible light and reacts with $^1O_2$. (ii) **RA** acts as a temporally-controlled $^1O_2$ sensing reagent under the longer wavelength (~700 nm) photosensitization. **RA** enters an intermediate state after capturing $^1O_2$ and does not become strongly fluorescent until it is exposed to UV, blue, or green light. (iii) **RA** acts as an efficient photosensitizer to generate $^1O_2$ under green light illumination. The spin-orbit charge transfer mediated intersystem crossing (SOCT-ISC) process achieves this function, and **RA** shows a potential cancer-killing effect on pancreatic cancer cells. The wavelength-switchable functionalities in **RA** offer to promise molecular tools to apply $^1O_2$ in a spatiotemporal manner.

Introduction

Singlet oxygen ($^1\Delta_g$)($^1O_2$) is a particular form of the oxygen molecule and is an essential member of the reactive oxygen species (ROS) family.[1,2] $^1O_2$ is an active intermediate in various chemical and biological reactions. For instance, $^1O_2$ is the primary substance that plays an essential role in photo-mediated oxidation reactions, including type II photoreaction in photodynamic therapy (PDT).[2,3] Uncontrolled production of $^1O_2$ causes undesirable degradation of materials and oxidative stress-induced progression of diseases in biology.[4–6] Towards full use of $^1O_2$, its detection, imaging, and generation have been active research areas.[4,7–11]

Regarding $^1O_2$ sensing, most of the recently developed $^1O_2$ sensing molecules are combinations of fluorophores and $^1O_2$ scavenger moieties like anthracene.[9,12–15] A general theory suggests fluorescence in such pristine sensor molecules is quenched because of photoinduced intramolecular electron transfer (PIET). The fluorescence appears when $^1O_2$ reacts with the scavenger molecule to form endoperoxide, suppressing the electron transfer. This strategy is widely used for fluorogenic sensors based on PIET in donor-acceptor (D-A) dyads for $^1O_2$ and other ROS.[9,12–15]

Recently, the electron-donating property of the aminomethyl anthracene moiety reported by our group has further developed the D-A-based $^1O_2$ sensing strategy.[14–16] Coumarin-aminomethylanthracene diads are still weakly fluorescent after capturing $^1O_2$ and forming an endoperoxide. Remarkably, an intense fluorescent property is triggered by an additional photoexcitation of the endoperoxide.[16] This phenomenon originates from the unique energy levels of photoexcited states and the nitrogen atom of the molecule, which accelerates the intersystem crossing most probably *via* the spin-orbit charge transfer mediated intersystem crossing (SOCT-ISC).[17] However, the reported coumarin dyads needed UV light for the phototriggered fluorescence activation, which may cause undesired cytotoxicity. Moreover, the poor solubility of coumarin dyads in aqueous solvents limits its bioapplication. These characteristics should be improved for further applications of the dyad system.

Meanwhile, regarding $^1O_2$ generation, SOCT-ISC in the D-A molecules has recently gathered much attention for photoinduced $^1O_2$ generation because it increases the efficiency of utilizing the triplet excited state energy.[17–19] Filatov and coworkers reported that anthracene-BODIPY molecules are good triplet photosensitizers because the charge separation energy level mediates a small singlet-triplet energy gap based on SOCT-ISC

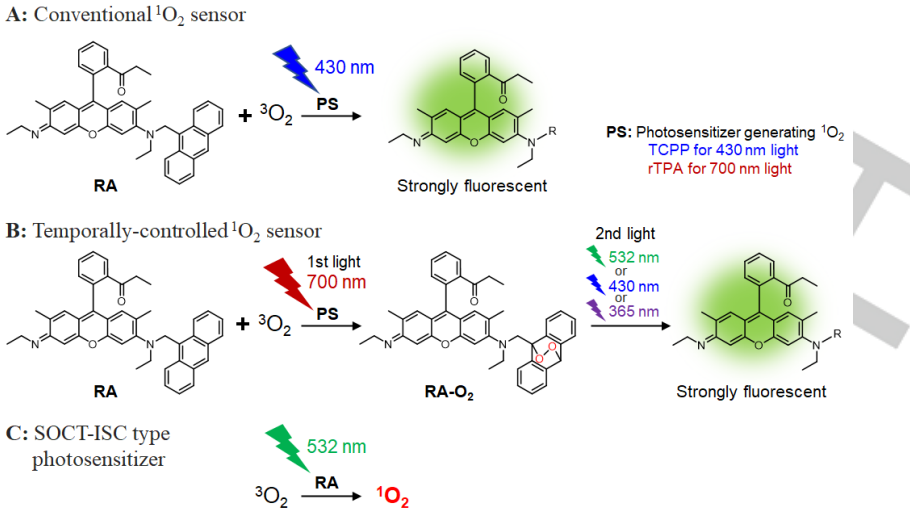

Scheme 1. Wavelength-dependent functions of the sensor **RA**. It acts as (A) a conventional $^1O_2$ sensor molecule under the light which RA absorbs, (B) a temporally-controlled $^1O_2$ sensor without the light which is absorbed by **RA** during $^1O_2$ capturtching, and (C) a SOCT-ISC type photosensitizer under the light which is absorbed by **RA**.

and efficient $^1O_2$ generation.[20] Because molecular systems using SOCT-ISC are still to be developed, a profound understanding of $^1O_2$ generation by SOCT-ISC molecules is fundamentally essential.

In this study, rhodamine 6G-anthracene linked molecule (**RA**) is designed, synthesized, and studied to reveal wavelength-dependent $^1O_2$ sensing/generating abilities. The positively charged amphiphilic rhodamine 6G analog of **RA** achieves water solubility and mitochondrial localization. **RA** acts as a fluorogenic $^1O_2$ sensing molecule like SOSG[21] under UV, blue, and green light illuminations. **RA** acts as the temporally controlled $^1O_2$ sensing reagent by long-wavelength phototriggering, such as NIR light. **RA** also acts as a photosensitizer based on the SOCT-ISC process. Such multifunctional molecules are advantageous for developing molecular tools for precise spatiotemporal controlling optical responses using engineered photoexcited states.

Results and Discussion

Design, synthesis, and characterization of the rhodamine 6G-anthracene conjugate (RA).

The rhodamine 6G moiety was employed to afford green light absorption and water-solubility of **RA**, and an anthracenyl moiety to afford the $^1O_2$ trapping ability of **RA**. **RA** was synthesized from rhodamine 6G and chloromethyl anthracene (see the supporting information for the synthetic details). After the purification, **RA** was characterized by spectroscopic methods, including ESI-mass and NMR. Figure 1 shows the absorption spectra of **RA** at various concentrations in ethanol, PBS, and DMF. Characteristic absorption bands of the anthracenyl and rhodamine moieties appeared around 370 and 540 nm, respectively. The molar absorption coefficients of **RA** in ethanol, PBS, and DMF were determined at 6.2×10^4, 8.3×10^4, and 2.5×10^4 L mol^{-1} cm^{-1} (Figure S1). The higher values in ethanol and PBS than DMF would reflect the influence of protonation on the absorption characteristics of the rhodamine moiety in **RA**.

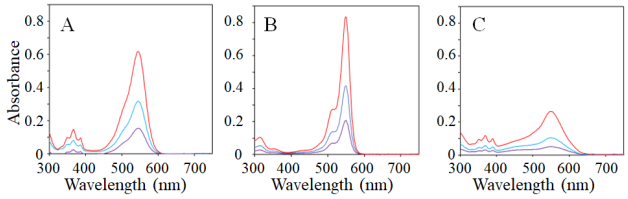

Figure 1. Absorption spectra of **RA** in (A) ethanol, (B) PBS, and (C) DMF with the concentrations (purple) 2.5, (blue) 5.0, (red) 10 μM.

Table 1. The first redox potentials of **RA**, [a] E_{00} values,[b] and the free energy charge of PIET.[c]

E_{ox} / V[a]	E_{red} / V[a]	$E_{0,0}$ / eV[b]	ΔG_{ET} / eV[c]
0.53	-1.16 V	2.26	-0.57

[a] Values of redox potentials are given in volts relative to $Fc^{0/+}$ redox couple and were obtained from differential pulse voltammetry in deaerated DMF. Conditions: glassy carbon electrode as a working electrode, the counter electrode was a platinum wire, and Ag/Ag^+ the reference electrode. [b] Obtained from the offset in the absorption spectra. c) Obtained from Eq. 1.

PIET between the donor and acceptor moieties in **RA** is essential for fluorescence quenching before trapping $^1O_2$. The thermodynamic feasibility of the PIET in **RA** was verified by estimating the free energy change of the process according to eq. 1;[22]

$$\Delta G(eV) = E_{ox} - E_{red} - E_{0,0} \quad \text{(eq.1)}$$

where E_{ox} is the first oxidation potential of the donor moiety, E_{red} is the first reduction potential of the acceptor, and $E_{0,0}$ is the zero-zero transition energy, as shown in Table 1. The negative Gibbs energy change (ΔG_{ET} = -0.57 eV) verifies an efficient PIET causing fluorescence quenching in **RA** before trapping $^1O_2$. As expected from the value, **RA** shows a weak fluorescence (Figure 2A).

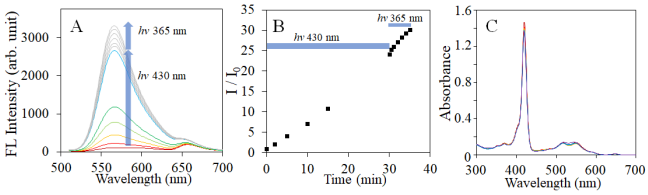

Figure 2. (A) Fluorescence spectra (λ_{ex}: 500 nm) of **RA** (2.5 μM) and TCPP (4.0 μM) in DMF before and after the 430 nm photosensitization (red to blue lines), followed by photoactivation by the UV illumination (365 nm, 1.0 mW cm^{-2}) (gray lines), (B) the corresponding time-traced relative fluorescence intensities at 560 nm, and (C) the corresponding absorption spectra.

Conventional fluorogenic $^1O_2$ sensing by RA.

We first checked the ability of **RA** as a conventional $^1O_2$ sensor molecule (Scheme 1A). A sample solution containing **RA** and TCPP as the photosensitizer in DMF or PBS was irradiated by a 430 nm blue light for the photosensitized $^1O_2$ generation by TCPP. The fluorescence intensity of **RA** was increased due to $^1O_2$ sensing through capturing $^1O_2$ (Figures 2A, B). **RA** showed 25-fold fluorescence enhancement after 30 min sensitization (Figures 2B and S2). The almost unchanged absorption spectra support no remarkable decomposition of **RA** (Figure 2C). Control experiments in the absence of TCPP confirmed that the increase in the fluorescence is not caused by the photodecomposition or self-sensitization of **RA** (Figure S3). 365 nm light illumination following the 430 nm photosensitization results in a similar trend of fluorescence increase (Figures 2A and 2B). This is a different change from that with 700 nm illumination, which will be discussed in the next section. These results indicate **RA** acts as a conventional fluorogenic $^1O_2$ reporter by UV~blue light excitation. High-performance liquid chromatography (HPLC) was performed to separate and identify the final products of the reaction of **RA** and $^1O_2$. ^{1}H-NMR spectra of the obtained mixture after the reaction indicated that one of the major products is anthraquinone (Figure S4D, E; signals at 8.22 and 7.96 ppm in DMSO). Anthraquinone is a typical product of the photoconversion of $^1O_2$ sensor molecules consisting of anthracene.[9,12–15] Therefore, the primary mechanism of the fluorescence enhancement would be the formation of the endoperoxide, **RA-O$_2$**, followed by the immediate cleavage of the anthracenyl part from **RA-O$_2$** (Scheme 1). The cleavage is probably triggered by the photoexcitation on the dye molecule, as discussed previously for a coumarin-anthracene conjugate[16] and below, enabling us to use photo-triggered temporally-controlled fluorogenic $^1O_2$ sensing by the molecules.

Phototrrigered temporally-controlled fluorogenic $^1O_2$ sensing by RA.

Our previous study showed that specific fluorophore-anthracene conjugates are not strongly fluorescent in their endoperoxide form after trapping $^1O_2$,[16] which contrasts sharply with the previously reported $^1O_2$ sensing molecules, such as SOSG.[23] The fluorophore-anthracene molecules become highly fluorescent once photoexcited after capturing $^1O_2$.[16] Based on this mechanism, we anticipated that **RA** possesses a similar characteristic, and the $^1O_2$ trapping by **RA** in the absence of the photoexcitation on **RA** can afford the weakly fluorescent endoperoxide **RA-O$_2$** (Scheme 1B). To evidence it, a π-extended porphyrin type photosensitizer, **rTPA**,[10] was employed because it efficiently absorbs 700 nm light where **RA** does not absorb. Upon continuous photoirradiation on a mixed solution of **RA** and **rTPA** at 700 nm (20 mW cm^{-2}), the fluorescence intensity of **RA** did not increase as quickly as that using TCPP with the blue light illumination discussed above (Figures 3A and 3B, red to blue traces until 30 min).

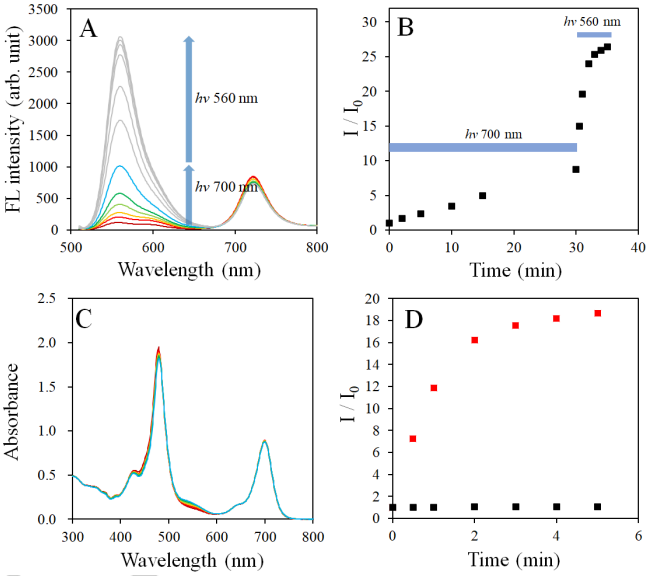

Figure 3. (A) Fluorescence spectra (λ_{ex}: 500 nm) of **RA** (5.0 μM) and **rTPA** (12.5 μM) in DMF before and after the 700 nm (20 mW cm^{-2}) photosensitization for 30 min (red to blue lines), followed by the photoactivation by the green light illumination (560 nm, 1.0 mW cm^{-2}) (gray lines), (B) the corresponding time-traced relative fluorescence intensities of **RA** at 560 nm and (C) the corresponding absorption spectra. (D) Time-traced relative fluorescence intensities of **RA** at 560 nm in the presence of **rTPA** during the green light photoactivation (560 nm, 1.0 mW cm^{-2}) (red plots) with or (black plots) without the primary 700 nm photosensitization.

The resultant solution was then illuminated with a relatively weak green light (560 nm, 1.0 mW cm^{-2}). Remarkably, the fluorescence intensity was quickly increased (Figures 3A and 3B). In contrast, green light illumination on **RA** without the prior photosensitization does not increase the fluorescence of **RA** (Figures 3D and S3). Therefore, the fluorescence enhancement was not caused by the decomposition or self-photosensitization by **RA** with the green light. Most probably, the endoperoxide form of **RA**, that is **RA-O$_2$**, is formed as in the case of the coumarin-anthracene conjugate.[16] Consequently, the photo-triggered fluorogenic $^1O_2$ sensing ability has been proved for **RA**. This dyad enables us to use temporally-controlled fluorogenic sensing of $^1O_2$.

We also found that the light source for the second illumination to photoexcite **RA-O$_2$** (Scheme 1) is not limited to the green light but also UV light (Table 2, Figures S5 and S6). Moreover, 15 min photosensitization by **rTPA** (Table 2 Entry 4) affords the best enhancement factor (= 3.14-fold) after the second illumination. Because the enhancement factor may depend on various factors, such as the electronic interaction in the molecules, further improvement is to be achieved by modifying or synthesizing new molecules. The most crucial point here is that **RA** enables us to use the green light for the phototriggered $^1O_2$ detection, which is more beneficial for further applications in chemistry and biology than UV and blue lights.

Table 2. Reaction conditions on the phototriggered fluorogenic $^1O_2$ sensing and the resulted enhancement factors of fluorescence in **RA**.

Entry	$^1O_2$ sensitizer	Solvent	1st light (20 mW cm^{-2})	2nd light (1.0 mW cm^{-2}, 5 min)	Enhancement factor in fluorescence after the 2nd light excitation[a]
1	TCPP	DMF	430 nm (30 min)	365 nm	1.24
2	**rTPA**	DMF	700 nm (30 min)	365 nm	2.81
3	**rTPA**	DMF	700 nm (60 min)	365 nm	1.84
4	**rTPA**	DMF	700 nm (15 min)	560 nm	3.14
5	**rTPA**	DMF	700 nm (30 min)	560 nm	3.02
6	**rTPA**	PBS	700 nm (90 min)	365 nm	1.51
7	**rTPA**	PBS	700 nm (30 min)	560 nm	1.56

[a] Calculated from the final fluorescence intensity after the 2nd light illumination divided by the fluorescence intensity just before the 2nd illumination.

The phototriggered $^1O_2$ sensing was also examined in an aqueous solution with the biological application in mind. A sample solution containing **RA** and **rTPA** in PBS was irradiated by the 700 nm light, followed by illumination by UV light (365 nm, 1.0 mW cm^{-2}) for photosensitization. Then, as in the case of DMF, a remarkable increase in fluorescence intensity was observed (Figures S2, S7, and S8). Thus, it was confirmed that the photo-triggered $^1O_2$ sensing is also present in an aqueous solution. Compared with our previously reported molecule, the water-insoluble coumarin-anthracene conjugate,[16] this result evidences the usability of **RA** to detect $^1O_2$ in an aqueous solution and a biological environment.

Density functional theory (DFT) calculations on RA.

DFT calculations were employed on **RA** and **RA-O$_2$** to understand the molecular structures and electronic properties causing the photo-triggered $^1O_2$ sensing by **RA**. The calculations at UB3LYP-D3/6-31G* level depicted the highest occupied molecular orbital (HOMO) and lowest unoccupied molecular orbital (LUMO) configuration in **RA** (Figure 4). The HOMO localizing on the anthracenyl moiety and the LUMO on the rhodamine moiety support the favorable PIET between the moieties through the orbitals.

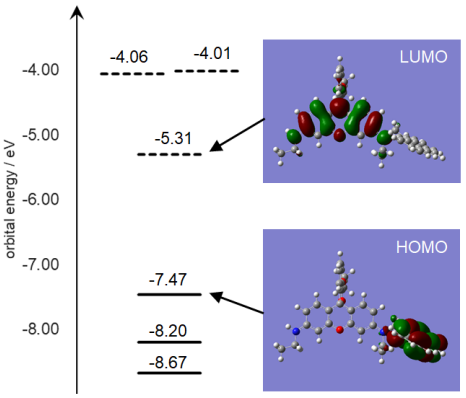

Figure 4. Calculated energy levels and orbital distributions of LUMOs and HOMOs of **RA** obtained by the DFT calculations at the UB3LYP/6-31^{++}G** level.

The energy level prediction by natural transition orbital (NTO) analyses on **RA** indicates that the transition from S_1 to T_3 states can be a major route for an ISC because of the small singlet-triplet energy gap. In addition, a charge-separated excited state in the singlet (S_{CSS1}) and triplet (T_{CSS1}) states have comparable energy levels. These features are favorable to achieving the SOCT-ISC process to obtain triplet excited states of the molecule efficiently.[17–19] Thus, **RA** can generate $^1O_2$ efficiently through the SOCT-ISC process (Figure 5).

Meanwhile, the NTO analysis on **RA-O$_2$** rationalizes its weak fluorescence. Because singlet-triplet transition pathways can be feasible, the radiative deactivation from the singlet excited state (=fluorescence) would be a minor pathway. Meanwhile, photoexcitation of **RA-O$_2$** may cause photocleavage of the anthraquinone or triplet-state generation, which was also observed on a coumarin-anthracene molecule.[16]

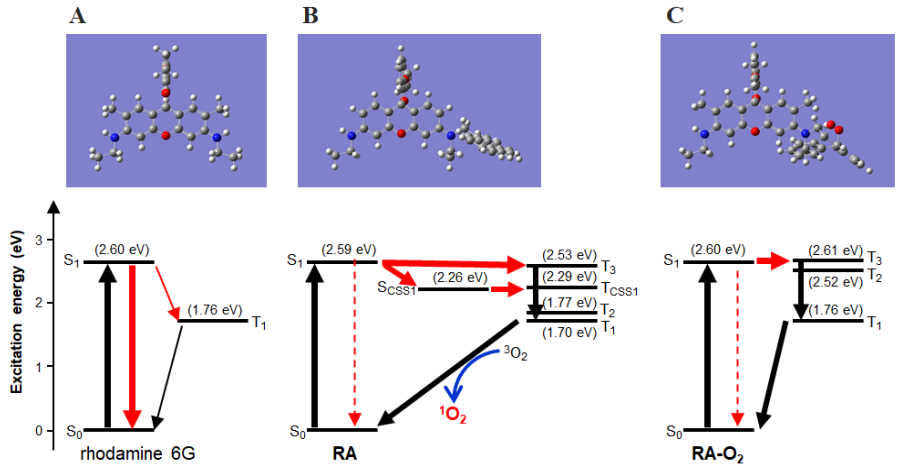

Figure 5. Optimized structures and energy levels predicted for (A) rhodamine 6G, (B) **RA**, and (C) **RA-O$_2$**, by the DFT calculations at the UB3LYP/6-31^{++}G** level with SCRF where DMF is the solvent. CSS denotes a charge-separated state.

$^1O_2$ generation by RA.

Encouraged by the DFT calculations indicating the SOCT-ISC, the $^1O_2$ generation ability of **RA** was examined. A direct comparison of the $^1O_2$ generation between **RA** and rhodamine 6G using SOSG reagent indicates that **RA** is more capable of generating $^1O_2$ than rhodamine 6G (Figure 6). The use of green light (560 nm, 20 mW cm^{-1}) rules out any direct contribution from the anthracenyl moiety, which cannot absorb the green light. Therefore, the unique electronic excited states of **RA**, as predicted by the DFT calculation, can offer the $^1O_2$ generation ability of **RA** based on the SOCT-ISC process. The quantum yield of $^1O_2$ photogeneration by **RA** was determined using Rose Bengal as the reference photosensitizer (Figures S9 and S10).[24] The obtained quantum yield is 0.33 for **RA**, which is 3-fold greater than rhodamine 6G (Φ_Δ = 0.10). Therefore, it was concluded that **RA** acts as a good photosensitizer to generate $^1O_2$ and the unique $^1O_2$ sensor molecule.

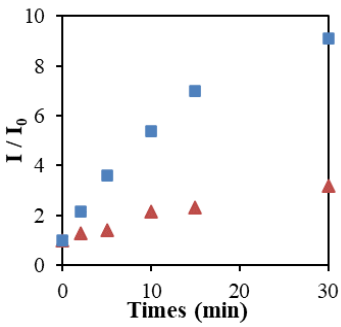

Figure 6. Time-traced $^1O_2$ generation indicated by the relative fluorescence intensities at 522 nm of SOSG (WL_{ex}: 450 nm) in 10 mM aq. HEPES with (blue square) **RA** or (red triangle) rhodamine 6G under green light illumination (560 nm, 20 mW cm^{-1}).

Spatiotemporal control on the photofunctionalities of RA. As mentioned above, **RA** is a unique $^1O_2$ sensor molecule and a photosensitizer depending on the light source. The photofunctinality of **RA** was examined in a spatiotemporally-controlled manner. First, a small portion of the mixed solution of **RA** and lipid molecules in ethanol was placed on a glass slide and dried. After the photoexcitation by a 488 nm laser, only the illuminated region enhanced the fluorescence signals (Figure S11). The fluorescence response of **RA** was recorded as the function of time under laser excitation (Figure S11D). The increase in the fluorescence response suggests the intracellular $^1O_2$ sensing is most probably by the self-sensitization of **RA**.

Next, the spatiotemporally controlled sensing ability of **RA** was examined in living cells. Remarkably, **RA** demonstrates a mitochondria-specific localization in HeLa cells, which are model cancer cells derived from cervical cancer cells. The dual-color confocal microscopy images provided information on the colocalization of **RA** in mitochondria stained by Mitotracker Deep Red dye (Figure 7). The Mander's colocalization coefficient for **RA** and Mitotracker Deep Red was found to be 0.88 ± 0.01,[20] referring to the very high mitochondrial targetability of **RA**.

It is noteworthy that the mitochondria-specific localization was also observed in pancreatic cancer cells (PCI-55 cells). Pancreatic cancer cells have recently gathered much attention in cancer therapy because of their aggressive feature and the low survival rate of the patients.[25] The time-lapse imaging with the focused laser excitation demonstrated the fluorescence enhancement from **RA** at the illuminated spot. The emerged green fluorescence would spread over only the illuminated cell (Figure 7E and the video in the supporting information). Moreover, the disappearance of the fluorescence of MitoTracker Deep Red in the illuminated cell indicates the effective cancer-killing, being reflected by the loss of mitochondrial membrane potential. The cell death is probably *via* a necrotic pathway because the swelling of the cells at the late stage of the photoexcitation was observed. This result indicates that **RA** shows the $^1O_2$ generating and detecting abilities spatiotemporally. It ensures that **RA** is a useful molecular tool to control and detect $^1O_2$ in a spatio-temporal selective manner.

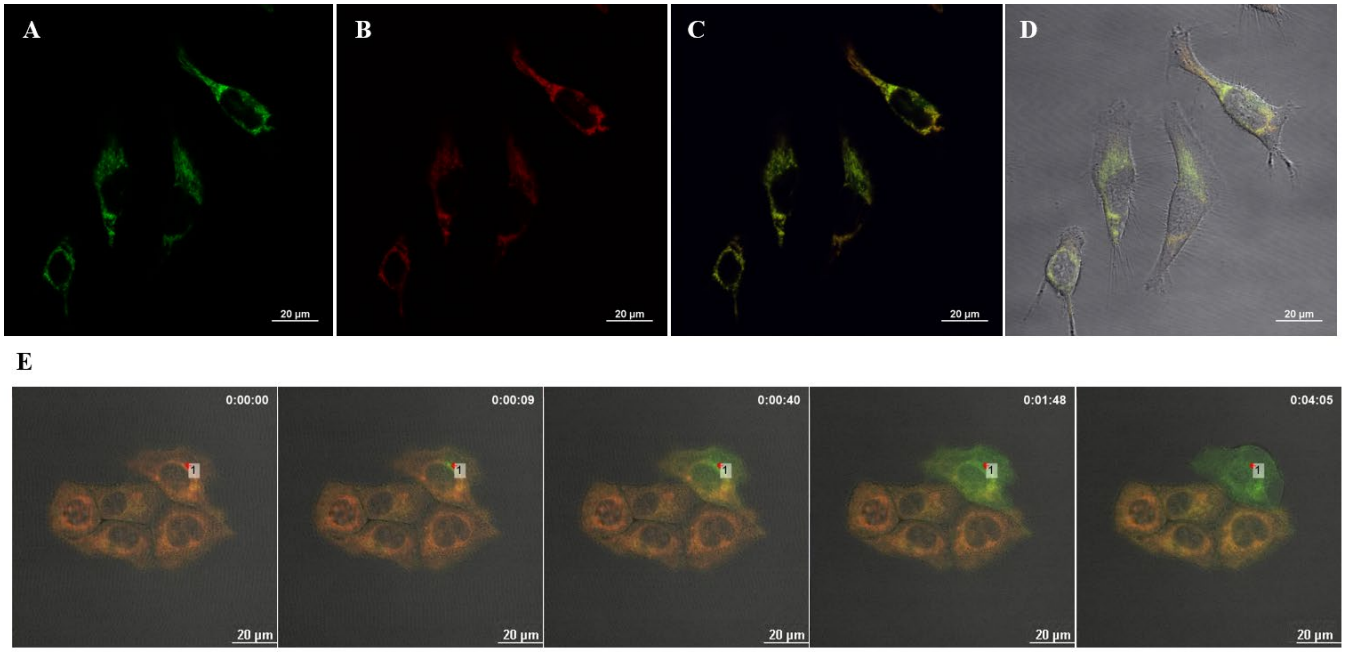

Figure 7. HeLa cells stained with (A) **RA** and (B) Mitotracker Deep Red, (C) their merged image, and (D) the overlay with a bright-field image. The yellow signals indicate the colocalization of **RA** and mitochondria. (E) PCI-55 cells stained with **RA** (green) and Mitotracker Deep Red (red) with a bright-field image at various time points with the focused laser excitation on a particular spot (shown as a red circle). The video is available as the supporting information.

Conclusion

A rhodamine 6G-anthracene-linked molecule, **RA**, demonstrated wavelength-dependent functionalities. **RA** acts as a conventional fluorogenic $^1O_2$ sensor molecule under the light which **RA** absorbs. **RA** acts as a temporally-controlled $^1O_2$ sensing reagent in the absence of blue and green light, which are not absorbed by **RA**. Or **RA** acts as a photosensitizer to generate $^1O_2$ via the SOCT-ISC process. Observations and DFT calculations explained well about the unique wavelength-dependent functionalities of **RA** based on its electronic structure. $^1O_2$ generation and sensing abilities of **RA** are also shown in a biological system, pancreatic cancer cells, with a potential cancer-killing effect. The presented strategy of the molecular design and the wavelength-switchable functionalities of **RA** pave the way to create multipotent and promising molecular tools to fully use $^1O_2$ in a spatiotemporal manner.

Experimental Section

General. Absorption and fluorescence spectra were recorded using a UV-vis spectrophotometer (Evolution 220, ThermoFisher Scientific) and a fluorescence spectrophotometer (Spectrofluorometer FL4500, Hitachi). ^1H and ^{13}C NMR spectra were measured using an Agilent Unity INOVA 500 or JEOL JNN-EX400 spectrometers. FT-IR spectra were recorded on a JEOL FT/IR 660Plus spectrometer. High-resolution ESI mass spectra were obtained with a ThermoFisher Scientific Exactive (ESI) system.

Conventional fluorogenic $^1O_2$ sensing by RA. The $^1O_2$ sensing ability of **RA** was studied using spectroscopic fluorescence techniques. $^1O_2$ was generated using a photosensitizer (PS), Tetrakis(4-carboxyphenyl)porphyrin (TCPP) for the 430 nm photosensitization. A sample solution containing 2.5 μM **RA** and PS in phosphate buffer saline (PBS) or DMF was irradiated by a 430 nm blue LED at 20 mW cm^{-2} (CL, Asahi-spectra co. Ltd., Japan) for TCPP for a $^1O_2$ generation. The absorption and fluorescence spectra of the sample solution were recorded at regular intervals.

Phototrrigered temporally-controlled fluorogenic $^1O_2$ sensing by RA. $^1O_2$ was generated using a photosensitizer (PS), **rTPA**, for the 700 nm photosensitization. A sample solution containing 5.0 μM **RA** and PS in PBS or DMF was irradiated (20 mW cm^{-2}) by a lamp equipped with a 700 nm ± 10 nm bandpass filter (LAX-C100, Asahi-spectra co. Ltd.,) for the photosensitized generation of $^1O_2$. The absorption and fluorescence spectra of the sample solution were recorded at regular intervals. After the photosensitization, the solution of **RA** and PS was further illuminated (1 mW cm^{-2}) by UV or green light from a lamp equipped with a 365 nm ± 10 nm or 560 nm ± 10 nm bandpass filter (LAX-C100, Asahi-spectra co. Ltd.,). Changes in the fluorescence intensity were recorded. As a control experiment, the mixture of the same composition was excited by the UV or green light without the prior photosensitization.

DFT calculations. Geometries of rhodamine 6G, **RA** and **RA-O_2** were optimized using the Gaussian 16 Revision D.01 program[26] with the B3LYP[27,28] functional with the D3 version of Grimme's dispersion and the original D3 damping function[29]. The 6-31G(d) [30] basis set was used. Molecular orbital analyses were performed with the natural transition orbitals (NTO).[31]

Acknowledgements

We acknowledge financial support from MEXT under the JSPS Grant-in-Aid for Scientific Research B (19H02550 to V.B, and 21H01753 to Y.T.), for Challenging Research (Exploratory) (21K19036 to Y.T.), the JSPS Core-to-Core Program for Advanced Research Network, the JSPS Photoexcitonix Program, and the JSPS Dynamic Alliance for Open Innovation Bridging Human, Environment, and Materials.

Keywords: cancer phototherapy • donor-acceptor • fluorescence • reactive oxygen species • singlet oxygen

[1] M. C. DeRosa, R. J. Crutchley, *Coord. Chem. Rev.* **2002**, *233–234*, 351–371.
[2] G. M. F. Calixto, J. Bernegossi, L. M. De Freitas, C. R. Fontana, M. Chorilli, A. M. Grumezescu, *Molecules* **2016**, *21*, 1–18.
[3] H. S. Jung, J. Han, H. Shi, S. Koo, H. Singh, H. J. Kim, J. L. Sessler, J. Y. Lee, J. H. Kim, J. S. Kim, *J. Am. Chem. Soc.* **2017**, *139*, 7595–7602.
[4] M. A. Filatov, E. Heinrich, D. Busko, I. Z. Ilieva, K. Landfester, S. Baluschev, *Phys. Chem. Chem. Phys.* **2015**, *17*, 6501–6510.
[5] J. M. Aubry, C. Pierlot, J. Rigaudy, R. Schmidt, *Acc. Chem. Res.* **2003**, *36*, 668–675.
[6] S. I. Yamashita, M. Hamada, S. Nakanishi, H. Saito, Y. Nosaka, S. I. Wakida, V. Biju, *Angew. Chem., Int. Ed.* **2015**, *54*, 3892–3896.
[7] W. Fudickar, T. Linker, *Angew. Chem., Int. Ed.* **2018**, *57*, 12971–12975.
[8] E. Ucar, D. Xi, O. Seven, C. Kaya, X. Peng, W. Sun, E. U. Akkaya, *Chem. Commun.* **2019**, *55*, 13808–13811.
[9] A. P. De Silva, T. S. Moody, G. D. Wright, *Analyst* **2009**, *134*, 2385–2393.
[10] Satrialdi, R. Munechika, V. Biju, Y. Takano, H. Harashima, Y. Yamada, *Chem. Commun.* **2020**, *56*, 1145–1148.
[11] Satrialdi, Y. Takano, E. Hirata, N. Ushijima, H. Harashima, Y. Yamada, *Nanoscale Adv.* **2021**, *3*, 5919–5927.
[12] S. Kim, T. Tachikawa, M. Fujitsuka, T. Majima, *J. Am. Chem. Soc.* **2014**, *136*, 11707-11715.
[13] S. Kim, M. Fujitsuka, T. Majima, *J. Phys. Chem. B* **2013**, *117*, 13985–13992.
[14] R. Kohara, K. Yuyama, Y. Shigeri, V. Biju, *ChemPhotoChem* **2017**, *1*, 299–303.
[15] D. Sasikumar, R. Kohara, Y. Takano, K. ichi Yuyama, V. Biju, *J. Chem. Sci.* **2019**, *131*, 131–136.
[16] D. Sasikumar, Y. Takano, H. Zhao, R. Kohara, M. Hamada, Y. Kobori, V. Biju, *Sci. Rep.*,2022, **12**, 11371.
[17] C. M. Marian, *Wiley Interdiscip. Rev.: Comput. Mol. Sci.* **2012**, *2*, 187–203.
[18] M. Hu, A. A. Sukhanov, X. Zhang, A. Elmali, J. Zhao, S. Ji, A. Karatay, V. K. Voronkova, *J. Phys. Chem. B* **2021**, *125*, 4187–4203.
[19] M. A. Filatov, S. Karuthedath, P. M. Polestshuk, H. Savoie, K. J. Flanagan, C. Sy, E. Sitte, M. Telitchko, F. Laquai, R. W. Boyle, M. O. Senge, *J. Am. Chem. Soc.* **2017**, *139*, 6282–6285.
[20] M. A. Filatov, S. Karuthedath, P. M. Polestshuk, H. Savoie, K. J. Flanagan, C. Sy, E. Sitte, M. Telitchko, F. Laquai, R. W. Boyle, M. O. Senge, *J. Am. Chem. Soc.* **2017**, *139*, 6282–6285.
[21] M. Garcia-Diaz, Y. Y. Huang, M. R. Hamblin, *Methods* **2016**, *109*, DOI 10.1016/j.ymeth.2016.06.025.
[22] S. I. Yamashita, M. Hamada, S. Nakanishi, H. Saito, Y. Nosaka, S. I. Wakida, V. Biju, *Angew. Chem., Int. Ed.* **2015**, *54*, 3892–3896.
[23] M. Garcia-Diaz, Y. Y. Huang, M. R. Hamblin, *Methods* **2016**, *109*, 158-166.
[24] I. F. A. Mariz, S. N. Pinto, A. M. Santiago, J. M. G. Martinho, J. Recio, J. J. Vaquero, A. M. Cuadro, E. Maçôas, *Commun. Chem.* **2021**, *4*, 142.
[25] M. Hidalgo, *N. Engl. J. Med.* **2010**, *362*, 1605–1617.
[26] D. J. F. M. J. Frisch, G. W. Trucks, H. B. Schlegel, G. E. Scuseria, M. A. Robb, J. R. Cheeseman, G. Scalmani, V. Barone, G. A. Petersson, H. Nakatsuji, X. Li, M. Caricato, A. V. Marenich, J. Bloino, B. G. Janesko, R. Gomperts, B. Mennucci, H. P. Hratchian, J. V., *Gaussian 16, Revision C.01*, Gaussian, Inc., 2016, Wallingford CT.
[27] A. D. McLean, G. S. Chandler, *J. Chem. Phys.* **1980**, *72*, 5639–5648.
[28] R. Krishnan, J. S. Binkley, R. Seeger, J. A. Pople, *J. Chem. Phys.* **1980**, *72*, 650–654.
[29] S. Grimme, J. Antony, S. Ehrlich, H. Krieg, *J. Chem. Phys.* **2010**, *132*, 154104.
[30] G. A. Petersson, A. Bennett, T. G. Tensfeldt, M. A. Al‐Laham, W. A. Shirley, J. Mantzaris, *J. Chem. Phys.* **1988**, *89*, 2193–2218.
[31] R. L. Martin, *J. Chem. Phys.* **2003**, *118*, 4775–4777.

Entry for the Table of Contents

Insert graphic for Table of Contents here.

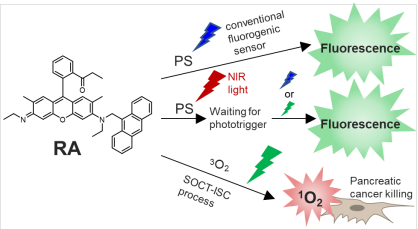

Rhodamine 6G-anthracene conjugate acts as a conventional $^1O_2$ sensor, a unique spatiotemporally controlled $^1O_2$ sensor, or a good photosensitizer depending on the photoexcitation wavelengths. Experimental results and DFT calculations suggest that the unique multifunctionality was achieved by the unique photoexcited states of the molecule. The molecular ability in living cells was also demonstrated.